Inorganic Chemistry

pubs.acs.org/IC Article

Investigations of Nanoparticle Suspensions of Prussian Blue and Its Copper Analogue: Amine Functionalization and Electrochemical Studies

Heshali K. Welgama, Matthew R. Crawley, James R. McKone, and Timothy R. Cook*



Cite This: Inorg. Chem. 2023, 62, 1455-1465



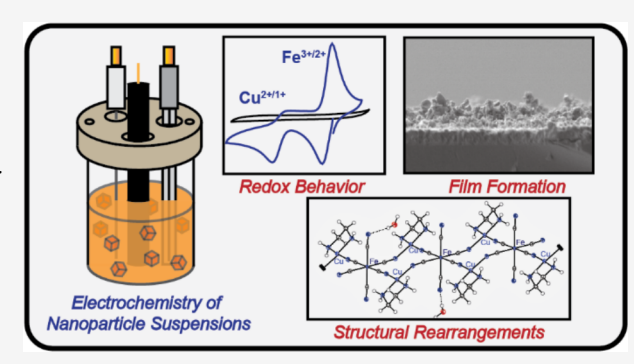
ACCESS I

Metrics & More

Article Recommendations

Supporting Information

ABSTRACT: Prussian blue (PB) and its analogues are promising materials for electrochemical energy storage, yet their use in flow-type devices is limited by their lack of redox responsiveness as colloidal suspensions. We have investigated the redox chemistry amine functionalization of PB along with its Cu analogue (CuPBA). No redox response of colloidal PB was observed and suspensions of CuPBA formed films on electrode surfaces with and without applied potentials; the films were redox-active but the material that remained suspended in solution did not participate in redox chemistry. Propylamine (pa), ethylenediamine (en), or tetramethylethylenediamine (TMEDA) were added in an attempt to maintain well dispersed suspensions through nanoparticle surface functionalization. Propyl-



amine modifications resulted in a loss of the CuPBA network and subsequent precipitation of insoluble materials. Coordination of ethylenediamine prompted the formation of Cu and Fe monomers ($[Cu(en)_2]^{m+}/[Fe(CN)_6]^{n-}]$) that remained soluble in aqueous electrolytes. In the absence of supporting electrolytes, these monomers formed a one-dimensional (1D) polymeric structure (Cu_2Fe_1D). TMEDA modification preserved the CuPBA extended structure with only modest precipitate formation over 30 min. The redox responsiveness of these suspensions depended on conditions; in 1 M KCl, no redox chemistry was observed for the CuPBA. In pH 4 potassium hydrogen phthalate buffer, a signal was observed that was attributed to the Fe centers of CuPBA. Under these conditions, the material precipitated in ~15 min and the signal was lost. Although the Fe centers in these networks are redox-active, additional work is needed to realize longer-term redox activity and stability. Ligand modifications can alter the properties of these networks but within a given ligand class, e.g., amines, the effects can vary greatly from the deconstruction of the framework to preventing film formation.

■ INTRODUCTION

Redox-active nanoparticles are attractive for electrochemical energy storage (EES), especially when immobilized or under heterogeneous conditions. In these schemes, nanoparticles are advantageous for their fast rates of charge transfer, short diffusion lengths, and potential for storing multiple equivalents of charge per nanoparticle. Formulations that are soluble or capable of forming colloidal suspensions are not as widely studied, despite the attractiveness of systems that translate the effective redox properties mentioned above to the solution phase where they could be used in redox flow batteries (RFBs).

Some significant prior work on suspensions of charge storage nanomaterials includes redox-active colloids based on polymers for nonaqueous flow batteries by Rodríguez-López and coworkers,⁵ hydrophilic redox-active polymer nanoparticles by Oyaizu and coworkers,⁶ nanoparticle suspensions of Li storage compounds by Tarascon and coworkers,⁷ as well as suspensions of conducting carbon nanoparticles for Li-based flow batteries by Chiang and coworkers.⁸ There are also a

handful of electroactive nanofluids based on graphene or metal oxides that can be pumped across stationary electrodes.⁹

Redox-active nanoparticles have also been used as a solid-phase component of RFBs alongside redox mediators to improve energy density, as in the case of metal oxides such as TiO₂ and Li⁺-storage compounds like LiFePO₄. We became interested in PB and its copper analogue (CuPBA), which have been used in RFBs, although not as colloidal suspensions. Kurihara and coworkers have previously shown that surface modifications can greatly alter the dispersibility of nanoscopic PB, although they did not explore any redox chemistry in the solution phase nor was this chemistry extended to CuPBA. Here, we study the coordination and redox chemistry of both

Received: October 6, 2022 Published: January 13, 2023





PB and CuPBA, with an emphasis on understanding the effects of adding amine ligands intended to alter the dispersibility and/or redox activity.

PB was first synthesized in the early 1700s, making it the first reported coordination polymer.¹³ Two recent perspectives, one by Ivanov, the other by Kraft, provide comprehensive background information on PB, invoking hundreds of years of research.¹⁴ PB consists of Fe(II) and Fe(III) metal centers that are bridged by cyano ligands. The Fe(II) centers are generally surrounded by carbon and the Fe(III) centers by nitrogen, as depicted in Figure 1. For a defect-free, idealized

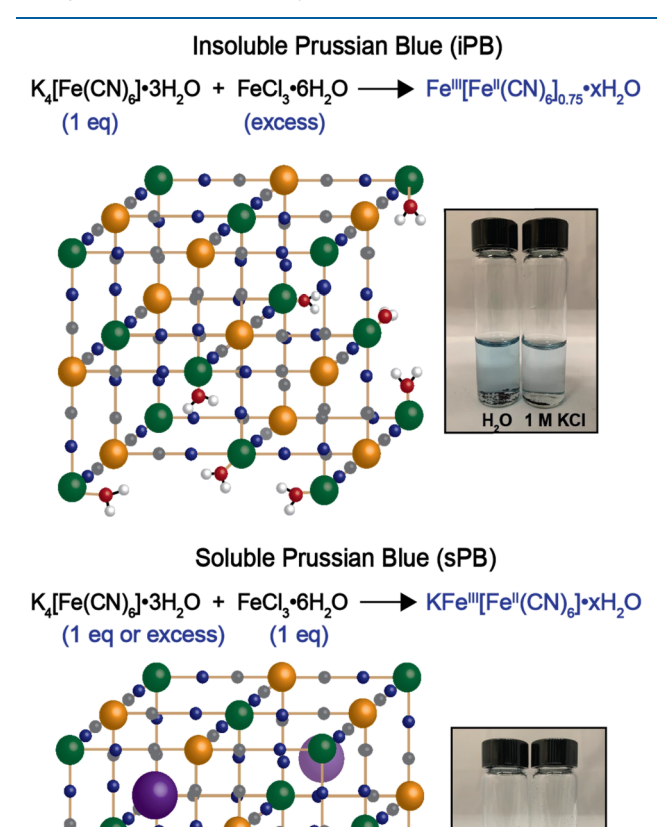


Figure 1. Synthetic routes to insoluble and soluble PB, which differ in their ability to form colloidal suspensions in water and 1 M KCl solutions.

▶ Fe³+ <mark>●</mark> Fe²+ • N • C **■** K+ 🔑 H,ูO

lattice, there are six cyanide ligands for every pair of Fe(II) and Fe(III) ions. Thus, the overall framework bears a negative charge and charge-compensating cations must occupy the interstitial voids. Under certain synthetic conditions, PB forms stable colloidal suspensions in water. This subset of PB is often called "soluble Prussian blue" (sPB) because these compounds form stable colloidal suspensions of nanoscopic particles in water. Other forms of PB balance the charge of the iron cations and cyanides through the introduction of vacancies in the hexacyanoferrate sites. ¹⁵ These charge-balanced frameworks do not form stable colloidal suspensions and have been described

as "insoluble Prussian blue" (iPB). Both frameworks contain interstitial water molecules, although the schematic representation in Figure 1 only shows those coordinated to Fe(III) centers in sPB for clarity. The Fe(II) and Fe(III) sites in PB are redox-active and their redox chemistry is accompanied by cation-intercalation/deintercalation. ¹⁶

PB has been extensively studied in heterogeneous films and composite electrodes. These studies have focused on PB's structural, ¹⁷ electrochemical, ¹⁸ magnetic, ¹⁹ electrochromic²⁰ properties, as well as on different applications of PB in catalysis, ²¹ electrochemical energy storage²² sensing, ²³ and selective adsorption. ²⁴ Nonetheless, little has been reported to date on the ability to access the redox chemistry of PB colloids. A recent study by Holdynski et al. reports on the electrochemistry of suspended PB nanoparticles using a rotating disk electrode, where sequential injections of PB yield stepwise increases in steady-state current flow. ²⁵ In another study, Cisternas et al. observe suspended PB forming a film on an electrode surface during cyclic voltammetry experiments. ²⁶

In this study, we explored the electrochemical behavior of aqueous PB colloids as well as CuPBA. We further modified these materials by introducing amines that caused a range of effects depending on the parent structure and the amine, including precipitation, dissolution to monomeric coordination complexes, topological rearrangement to alternative coordination polymers, and in one case, a redox-active suspension, although under these conditions, the material rapidly precipitated.

EXPERIMENTAL SECTION

Safety Note. Although the cyanide ligands in PB and CuPBA are generally inert, under acidic conditions, these materials can evolve HCN, for instance, during acid-digestions for analysis. Thus, these materials are most safely handled in small amounts in a fume hood and care must be taken to avoid the introduction of acid.

Materials. Potassium ferricyanide 99 + % (Acros Organics), potassium ferrocyanide 99 + %, cupric nitrate 2.5 hydrate (J.T. Baker), propylamine 99 + % (Acros Organics), ethylenediamine 99% (Alfa Aeser), and $N_iN_iN_i'$, N_i' -tetramethylethylenediamine 99% (Alfa Aeser). All chemicals, reagents, and solvents were used without further purification unless otherwise specified. Milli-Q water with a resistivity of 18.2 M Ω was purified from a Milli-Q Gradient A10 water purification system.

Characterization. Fourier transform infrared (FTIR) spectra were acquired from a PerkinElmer 1760 FTIR spectrometer with attenuated total reflectance (ATR) using powdered samples. ATR and baseline corrections were done for all measurements. Powder X-ray diffraction (PXRD) patterns were collected from a Rigaku Ultima IV X-ray diffractometer equipped with a Cu source and operated at 1.76 kW power (40 kV, 44 mA). Diffraction patterns were measured over a 2θ range of $5^{\circ}-80^{\circ}$ at a scan rate of 2° min⁻¹. Single crystal X-ray diffraction (SXRD) data were collected on a Rigaku XtaLAB Synergy diffractometer with a PhotonJet Cu microfocus source, HyPix-6000HE Hybrid Photon Counting (HPC) detector, and an Oxford 800 cryostream at 100 K. Structure solution was performed using SHELXT on Olex2 software package. Scanning electron microscopy (SEM) images were acquired using a Carl Zeiss AURIGA electron microscope. All samples imaged with SEM were gold-coated with using a sputter coater system (SPI Module) for 30 s. UV-visible spectra were obtained using an Agilent Cary 8454 UV-visible spectrophotometer and a quartz cell with a 1 cm path length. Fe-Cu ratios of CuPBA and ($[Cu(en)_2]^{m+}/[Fe(CN)_6]^{n-}]$) were measured using a ThermoElectron X Series 2 inductively coupled plasma mass spectrometry (ICP-MS). For sample digestion, 2.8 mg of CuPBA and 1.33 mg of $[Cu(en)_2]^{m+}/[Fe(CN)_6]^{n-}$ were dissolved separately in 5 mL of Milli-Q water. Each sample (10 μ L) was added to separate 1-

dram vials along with 990 μL of 50:50 (v/v) metal-free HNO $_3-H_2O$ mixture and left for 4 days at room temperature. They were then diluted to 10 mL, giving a 2% HNO $_3$ final concentration. Calibration curves were prepared from 0–100 ppb for Fe and 0–150 ppb for Cu standards for quantification. Cobalt was used as the internal standard. The PlasmaLab software was used for data analysis.

Electrochemical Characterization. All electrochemical experiments were carried out at room temperature following a 20-minute nitrogen purge. A BioLogic SP-200 potentiostat/galvanostat and the EC-Lab software were used for data collection. Cyclic voltammetry (CV) experiments were recorded using a 3.0 mm diameter glassy carbon (CH instruments, USA) or an FTO glass (50 mm × 10 mm × 2.2 mm, Millipore Sigma) working electrode, an Ag/AgCl (3 M KCl) reference electrode (Pine research, USA), and a platinum wire counter electrode (CH instruments, USA). Cyclic voltammograms were carried out in 8 mL of 1 M potassium chloride (LabChem) solutions in Milli-Q water or pH 4 buffer solutions of potassium hydrogen phthalate (J.T. Baker). Current responses were converted to current densities using the geometric surface areas of the electrodes. All bulk electrolysis experiments were carried out in a glass H-cell (Adams and Chittenden, USA) with the two compartments separated by a glass frit (porosity $10-16 \mu m$). Each compartment was filled with 15 mL of solution. The working electrode was either a 3.0 mm glassy carbon disk, a graphite felt (10 mm × 10 mm × 3 mm, Fuel Cell Store), or a section of FTO glass (50 mm \times 10 mm \times 2.2 mm, Millipore Sigma). An Ag/AgCl (3 M KCl) reference electrode was placed in the same compartment as the working electrode and a platinum wire counter electrode in the opposite compartment completed the three-electrode configuration. The potential was held at 0.4 V vs Ag/AgCl (3 M KCl) for the bulk reduction of CuPBA and solutions were stirred throughout.

Heterogeneous films for CV studies were prepared following a literature procedure. The Carbon black (Beantown Chemical) (5.4 mg), 10 mg of the active material ([Cu(en)_2]^m+/[Fe(CN)_6]^n- or TMEDA-CuPBA), 100 μ L of ethanol, and 500 μ L of methylene chloride were mixed and sonicated for 1 h. Next, the solvent was evaporated and 70 μ L of Nafion dispersion (5% w/w in water/1-propanol mixture, Beantown Chemical) and 600 μ L of ethanol were added and sonicated for 1 h. Then, two 2 μ L aliquots of the ink were pipetted onto a glassy carbon electrode (the second drop was added after the first drop dried completely) and allowed to air-dry before running CV experiments.

Synthesis of iPB. The synthesis of iPB was adapted from a known procedure. 22a FeCl₃•6H₂O (0.2703 g, 1.000 mmol) was added to 20 mL of Milli-Q water. This solution was added dropwise into an 80 mL aqueous solution of K₄[Fe(CN)₆]•3H₂O (0.2114 g, 0.5004 mmol) while stirring. The dark blue solution obtained was stirred for 2 more hours and allowed to sit for 24 h at room temperature. The resulting dark blue precipitate was collected by centrifugation and washed thoroughly with Milli-Q water and ethanol. The solid was dried under vacuum at 80 °C for 16 h and stored in a desiccator. The final product was characterized by PXRD and SEM.

Synthesis of sPB. The synthesis of sPB followed a modified procedure from the literature. ^{22a} A 20 mL aqueous solution of $FeCl_3 \bullet 6H_2O$ (135.2 mg, 0.5002 mmol) was added dropwise into a 20 mL aqueous solution of $K_4[Fe(CN)_6] \bullet 3H_2O$ (211.3 mg, 0.5004 mmol) while stirring. The dark blue mixture was stirred for 2 more hours and allowed to sit for 24 h at room temperature. The solvent was removed using rotary evaporation. The solid was dried under vacuum at 80 °C for 16 h and stored in a desiccator. The final product was characterized by PXRD and SEM.

Synthesis of CuPBA. CuPBA was synthesized by a coprecipitation method adapted from a reported procedure. ²⁸ Aqueous solutions (48 mL each) of $Cu(NO_3)_2 \bullet 2.5H_2O$ (1116.6 mg 4.801 mmol, 0.1 M) and $K_3[Fe(CN)_6]$ (790.5 mg, 2.400 mmol, 0.05 M) were simultaneously added dropwise into 24 mL of Milli-Q water while stirring. The resulting brown colloidal suspension was sonicated for 20 min and allowed to sit for 6 h. The product was collected by centrifugation and washed three times with Milli-Q water. It was then

dried under vacuum at room temperature and stored in a desiccator. The product was characterized by PXRD, SEM, and FTIR.

Surface Modification of CuPBA with Amines. Surface modification was carried out by adapting a reported procedure. Forty-two milligrams (0.13 mmol of Cu based on the nominal formula $KCu[Fe(CN)_6]$ of CuPBA) were combined with 1 mL of Milli-Q water and sonicated, then stirred until no more solid particles were observed at the bottom of the reaction vessel when allowed to stand for a few seconds. A 1:10 v/v mixture of the amine (18.2 mmol, \sim 1.5 mL) and n-butanol was added to the CuPBA dispersion, and the reaction mixture was stirred for 24 h, during which time it turned purple. The product, a purple solid, was collected by centrifugation, washed with diethyl ether three times, and dried under vacuum at room temperature. The product was characterized by FTIR and PXRD.

Synthesis of [Cu(OH₂)Cl(en)₂]Cl. The synthesis was adapted with slight modifications from a previous procedure. ²⁹ CuCl₂•2H₂O (735.3 mg, 5.002 mmol) was dissolved in 5 mL of Milli-Q water. Ethylenediamine (0.674 mL, 10.0 mmol) was added dropwise into the CuCl₂ solution and the purple reaction mixture was stirred overnight at room temperature. Dark purple needle-like crystals were obtained by adding the mixture dropwise into a mixture of ethanol and ether. The product was characterized by SXRD and the unit cell data matched a previously reported structure with the given formula.

RESULTS AND DISCUSSION

Prussian Blue. The syntheses of sPB and iPB were straightforward and carried out using a 1:1 or 2:1 ratio of the Fe(III) precursor to $[Fe(CN)_6]$, respectively. In the PXRD pattern of iPB, we observed matches that are reported in the literature. The PXRD data for sPB are similar but contains additional peaks that correspond to KCl that forms as a byproduct from the synthesis (see Figure S1). SEM images and DLS data confirmed that both iPB and sPB have particle sizes in the nano-range (\sim 60 nm, see Figures S2 and S3). The photographs in Figure 1 show that the as-synthesized sPB readily forms suspensions, in contrast to iPB.

CV was used to study the redox reactivity of sPB and iPB suspensions. Most of the iPB did not disperse in 1 M KCl and settled at the bottom of the cell, as shown in Figure 1. We were unable to observe any redox signal for suspensions of iPB (see Figure S4) despite the fact that immobilized PB has two characteristic redox events, one for each of the distinct Fe centers. sPB did form a stable colloidal suspension, as evidenced by its uniform and intense blue appearance, but we again did not observe any redox signal attributable to framework Fe. Instead, the redox response of sPB suspensions (Figures S4 and S5) was assigned to a mixture of residual Fe(II) and Fe(III) [Fe(CN)₆]ⁿ⁻ monomers that could not be easily separated from the sPB.

CupBA. Since no redox response was observed for suspended sPB, we were curious if related frameworks may behave differently. Thus, we synthesized the Cu analogue for subsequent investigations. The redox behavior of a colloidal suspension of CuPBA in a 1 M KCl solution was studied using CV. Two redox events corresponding to Fe(III/II) and Cu(II/I) were observed (see Figure 2). The response observed was similar to those reported in the literature for CuPBA in heterogeneous films. The Fe(III/II) redox couple with an $E_{1/2}$ of 0.748 V vs Ag/AgCl (3 M KCl) is the redox event of focus when CuPBA is used in battery applications. 28

Upon further investigation, the redox responses of the CuPBA were found to result from a thin film that formed on the electrode surface. The presence of a film was confirmed after rinsing a glassy carbon working electrode with fresh

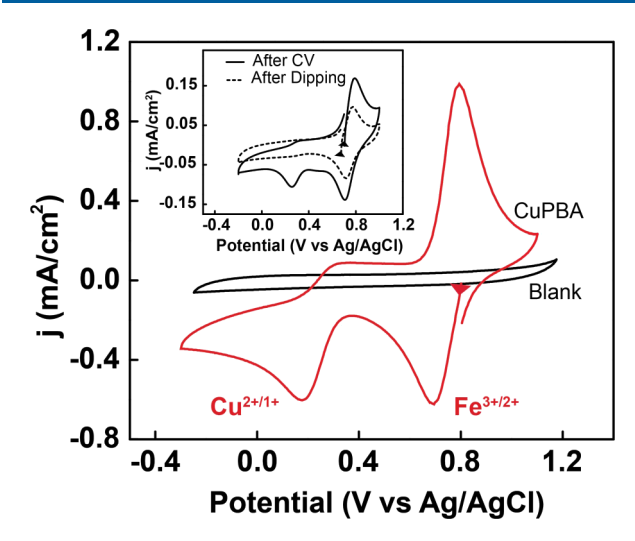


Figure 2. Cyclic voltammogram of a 10 mg/mL CuPBA suspension in 1 M KCl at 100 mV/s. Inset: Cyclic voltammograms in 1 M KCl show the film formation by suspended CuPBA in 1 M KCl on a glassy carbon working electrode, in the presence (solid line) and absence (dashed line) of a potential. The open circuit potential and scanning direction is shown by the arrowhead.

electrolyte solution, after running a CV in a suspension of CuPBA. The electrode was then placed in fresh 1 M KCl solution and another CV was collected. Although no film was apparent by visual inspection, a CV in 1 M KCl with no CuPBA showed a redox response (see inset of Figure 2), suggesting that a very thin layer of redox-active CuPBA still remained on the electrode surface.

It has been established that the voltammetric peak current for an immobilized film tends to increase linearly with the scan rate, whereas voltammograms that depend on diffusive reactant/product transport will vary linearly with the square root of the scan rate. Figure S8 shows that for our CuPBA film, the current response is more linear when plotted against the square root of the scan rate. We ascribe this response to the diffusion/intercalation of potassium ions that occurs when the film is redox-cycled rather than diffusion of the colloidal particles in solution. Bulk electrolysis experiments carried out at 0.4 V vs Ag/AgCl on the film take only seconds to plateau to negligible steady-state current, indicating that redox chemistry is largely confined to the surface and does not extend to the bulk solution (see Figure S9).

Upon extended CV cycling of a glassy carbon electrode in CuPBA suspension, we further observed a progressive increase in current response attributable to the Fe(III)/Fe(II) redox

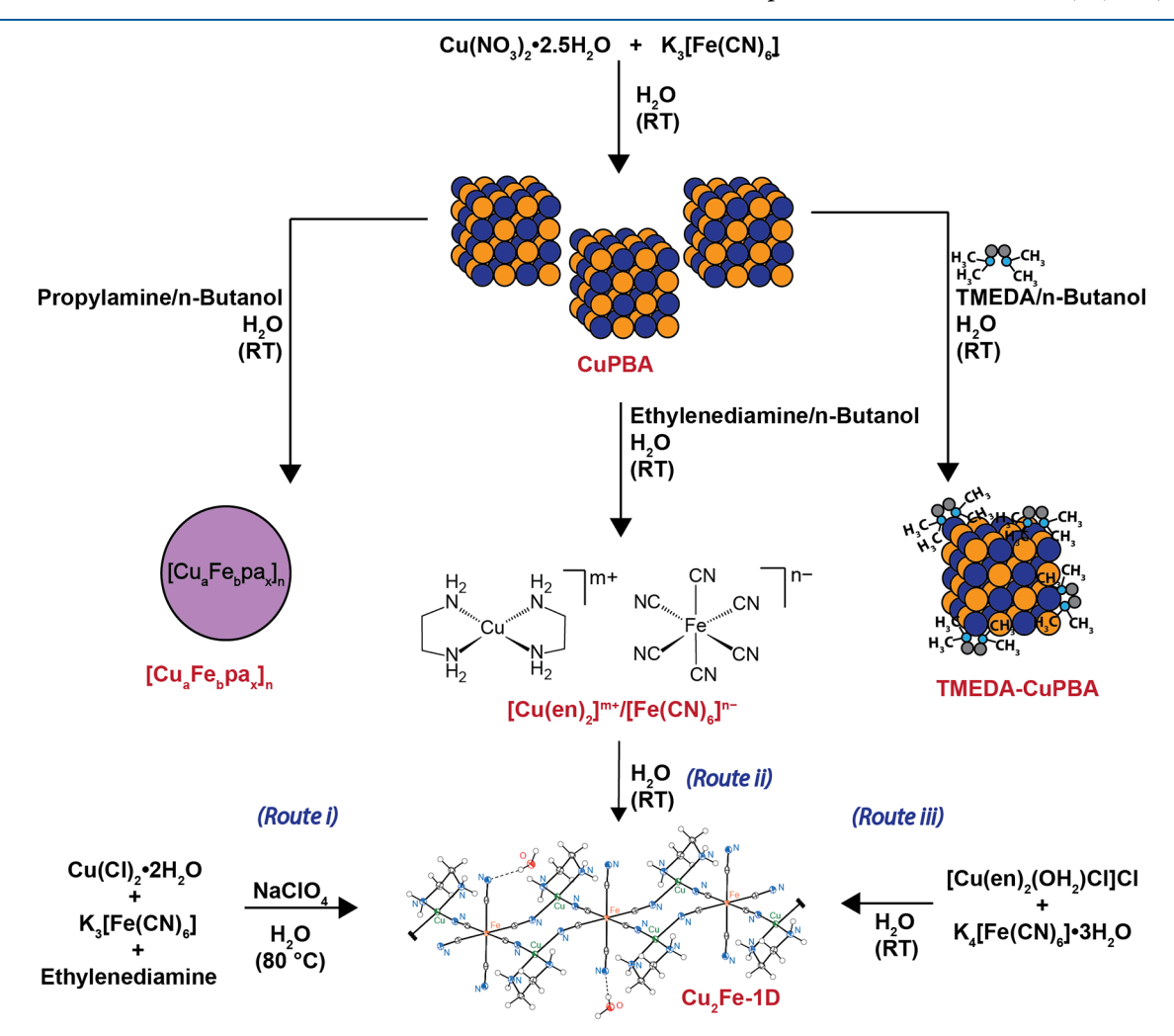


Figure 3. CuPBA synthesis and its surface modification using propylamine (pa), ethylenediamine (en), and tetramethylethylenediamine (TMEDA) along with subsequent transformations of these materials/compounds.

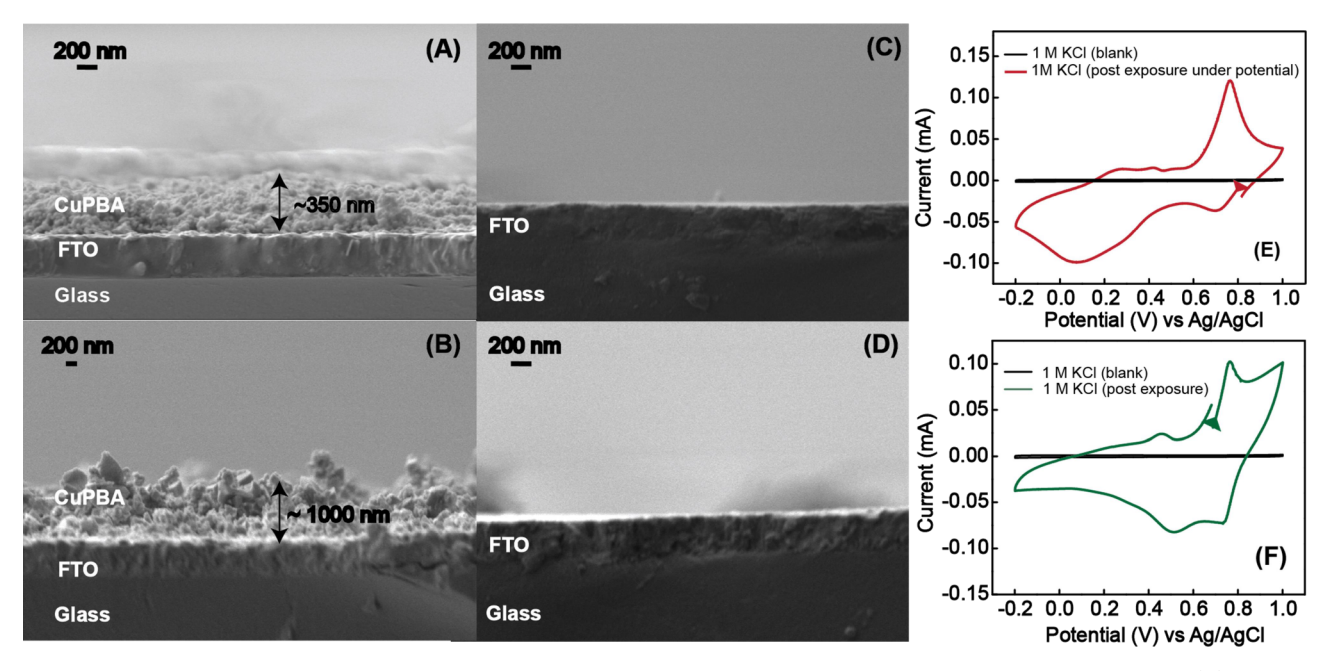


Figure 4. SEM of an FTO electrode cross-section after performing bulk reduction of a CuPBA suspension at 0.4 V vs Ag/AgCl for (A) 10 min and (B) 5 h. (C) and (D) FTO surface dipped in a CuPBA suspension in 10 min and 5 h, respectively. (E) Cyclic voltammograms in a 1 M KCl solution using a FTO working electrode after running a CV in a CuPBA suspension and (F) after dipping the FTO electrode for 60 s in a CuPBA suspension. Open circuit potential marked by arrowheads.

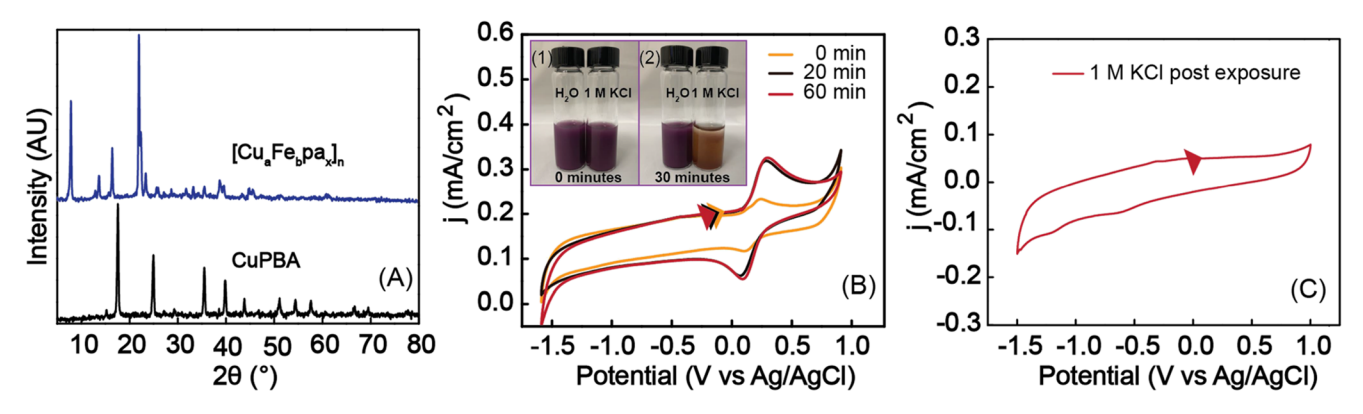


Figure 5. (A) PXRD of CuPBA before and after modification with propylamine, (B) cyclic voltammograms of a suspension of $[Cu_aFe_bpa_x]_n$ in 1 M KCl, and (C) of the electrode after washing and replacing with electrolyte solution containing no CuPBA,

couple with each cycle. Since we do not see any significant charge transfer to/from the bulk suspension, we conclude that this increased signal is due to growth in film thickness that increases the number of immobilized Fe sites. We explored this further on FTO electrodes as discussed below.

The formation of films from suspended PB has been observed before; however, notably, those films only start to show redox response after multiple cycles or on rotating electrodes that faciliate mass transport, whereas we see the CuPBA response on the very first CV sweep. Similarly, when a glassy carbon electrode was immersed in a CuPBA suspension in 1 M KCl for 60 s without any bias and a subsequent CV was run in fresh solution, a redox response consistent with a film was observed (see inset of Figure 2). Makowski et al. reported a similar CuPBA film formation by dipping a glassy carbon electrode in a solution containing $K_3[Fe(CN)_6]$, $CuSO_4$, and K_2SO_4 for 1 h. Sob As seen in both the cyclic voltammograms in the inset of Figure 2, the open circuit potential (OCP) shows that there is a partial reduction of Fe(III) into Fe(III) in the CuPBA film. Oxidized CuPBA can

promote water oxidation at this pH, resulting in partial reduction of the material. 32

We also studied CuPBA film formation on an FTO electrode surface to facilitate ex-situ electron microscopy. Using an FTO electrode as the working electrode, two bulk electrolysis experiments were carried out over 10 min and 5 h, respectively (Figure S10). Our objective was to observe the dependence of the film thickness on the time of exposure. Postelectrolysis, the FTO electrode was rinsed with Milli-O water and allowed to dry prior to SEM analysis. As shown in Figure 4A,B, the thicknesses of the films were approximately 350 and 1000 nm for 10 min and 5 h of bulk electrolysis, respectively. The rate of increase in film thickness therefore decreases with time, suggesting that the electrode surface is passivated by film formation. No film formation was observed by SEM when the electrode was simply dipped in a suspension of CuPBA in 1 M KCl, as shown in Figure 4C,D. Nonetheless, independent CV experiments (Figure 4E,F) did indicate that a CuPBA film does form on FTO upon completing a single CV sweep or simply dipping the electrode in CuPBA suspension. In both cases,

CVs in fresh KCl (aq) showed a redox event with an $E_{1/2}$ of 0.75 V vs Ag/AgCl. We also observe a difference in OCP between these two electrodes which suggests that the film exposed to a CV cycle during deposition contains more Fe(III) ions.

 $[Cu_aFe_bpa_x]_n$. To prevent film formation, we hypothesized that the modification of the PBA surface may disrupt aggregation of the particles. Thus, we exposed CuPBA to each of three amines, as shown in Figure 3. Propylamine was our first choice as a surface modifying ligand as there is a reported procedure using propylamine to make dispersible PB.¹²

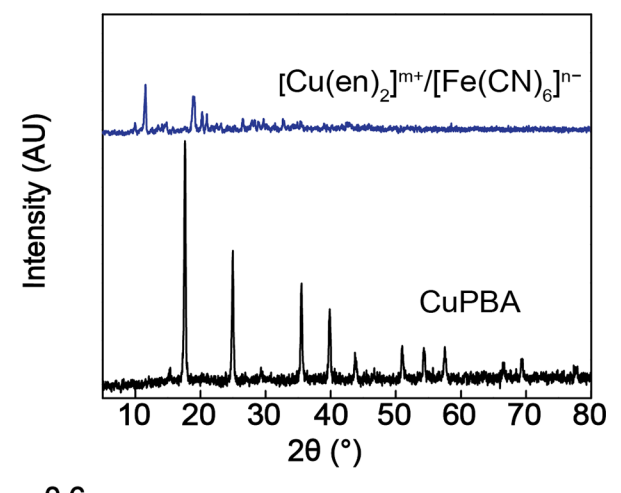
PXRD data showed that the initial CuPBA structure was lost after propylamine modifications (Figure 5A). The resulting $[Cu_aFe_bpa_x]_n$ material formed a purple-colored suspension in both water and 1 M KCl solution after sonication. However, within a period of 30 min in 1 M KCl, this $[Cu_aFe_bpa_x]_n$ started to precipitate and the color changed from purple to brown, as shown in Figure 5B. As expected, the CV showed no evidence for CuPBA and instead showed a redox response that corresponded to $[Fe(CN)_6]^{4-}$. Figure 5B also shows how the current response for $[Fe(CN)_6]^{4-}$ increased from 0 min (immediately after mixing) to 20 min and did not vary as much thereafter. After 60 min, all the materials precipitated, and there was no evidence for film formation on the glassy carbon working electrode (Figure 5C).

 $[Cu(en)_2]^{m+}/[Fe(CN)_6]^{n-}$. To assess whether a chelating amine would show similar behavior to propylamine, we also treated CuPBA with ethylenediamine. Here too, the PXRD data showed that the CuPBA framework did not persist. Unlike in the case of propylamine, this modified material remained well dispersed in 1 M KCl, giving rise to a clear purple-colored solution (see Figure S13). Subsequent experiments on this material established that the ethylenediamine prompts the formation of a mixture of mononuclear Cu and Fe complexes, which we abbreviate as $[Cu(en)_2]^{m+}/[Fe(CN)_6]^{n-}$.

To establish this chemistry, we carried out CV studies of $[Cu(en)_2]^{m+}/[Fe(CN)_6]^{n-}$ that showed a diagnostic redox response corresponding to $[Fe(CN)_6]^{4-}$ (Figure 6). Diffusion coefficients were calculated using the Randles–Sevcik equation along with data from a scan rate study for both $[Cu(en)_2]^{m+}/[Fe(CN)_6]^{n-}$ and $K_4[Fe(CN)_6]$ (Figure S14 and Table S1). If the reaction runs for lesser than 24 h, this material can be isolated in the $[Fe(CN)_6]^{3-}$ state (Figure S15). Longer reaction times result in more $[Fe(CN)_6]^{4-}$.

To elucidate the coordination environment of Cu, a bisethylenediamine Cu complex was synthesized from hydrated CuCl₂ and ethylenediamine. The unit cell data obtained from single crystals of this complex matched with that for the reported structure of $[Cu(OH_2)Cl(en)_2]Cl$. An aqueous solution of this complex possessed the same purple color as $([Cu(en)_2]^{m+}/[Fe(CN)_6]^{n-}$ in 1 M KCl (see Figure S13). UV–visible spectroscopy provided further evidence that surface modifications with ethylenediamine ultimately deliver Cu and Fe mononuclear complexes (see Figure 7). The spectral features of an aqueous mixture of the two mononuclear complexes, $K_4[Fe(CN)_6]$ and $[Cu(OH_2)Cl(en)_2]Cl$, were very similar to those of $[Cu(en)_2]^{m+}/[Fe(CN)_6]^{n-}$ in 1 M KCl solution.³³

When $[Cu(en)_2]^{m+}/[Fe(CN)_6]^{n-}$ is dissolved in Milli-Q water and allowed to sit at room temperature, within several days, brown crystals were observed. The solved structure was of a 1D polymer chain (Cu_2Fe-1D) with a Cu(II) and Fe(II)



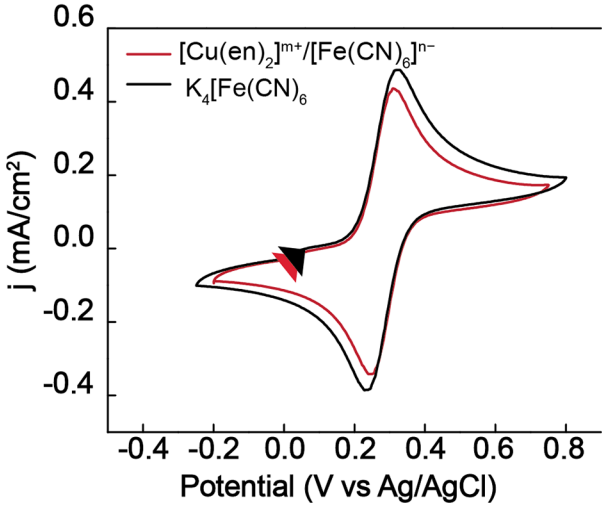


Figure 6. (top) PXRD of CuPBA before and after modification with ethylenediamine, cyclic voltammograms of 1 mg/mL. (bottom) $[Cu(en)_2]^{m+}/[Fe(CN)_6]^{n-}$ and $K_4[Fe(CN)_6]$ in 1 M KCl at 100 mV/s.

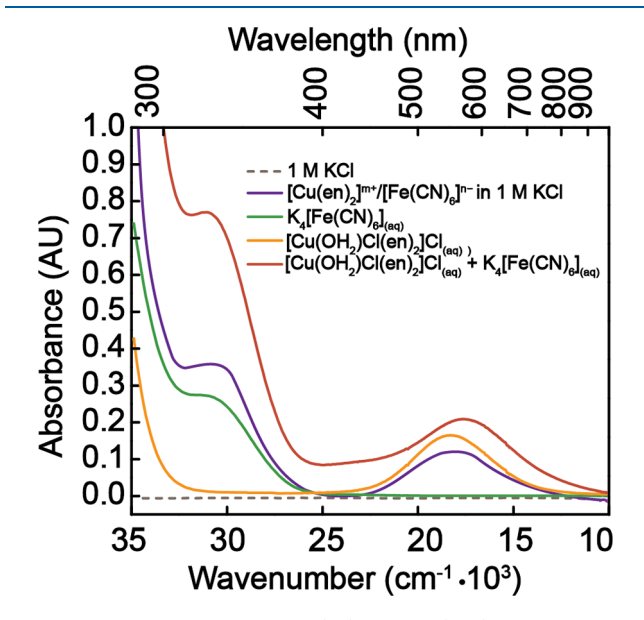


Figure 7. UV—vis spectra of $[Cu(en)_2]^{m+}/[Fe(CN)_6]^{n-}$ in 1 M KCl compared to aqueous solutions of mononuclear complexes $K_4[Fe(CN)_6]$ and $[Cu(OH_2)Cl]Cl$.

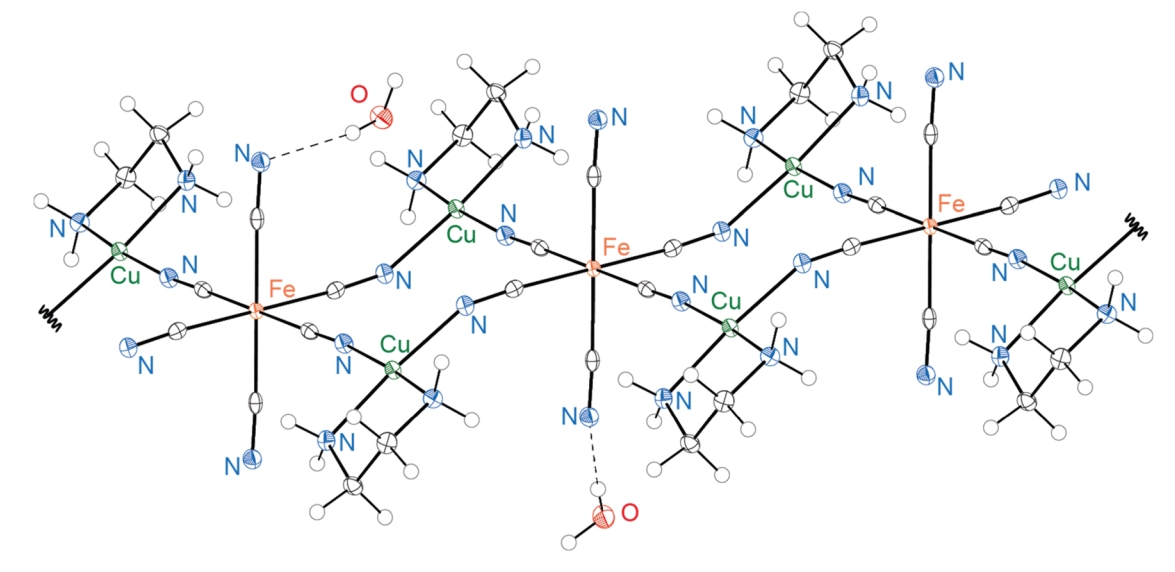


Figure 8. Crystal structure of the 1D polymer chain (Cu_2Fe-1D) formed from standing aqueous solutions of $[Cu(en)_2]^{m+}/[Fe(CN)_6]^{n-}$.

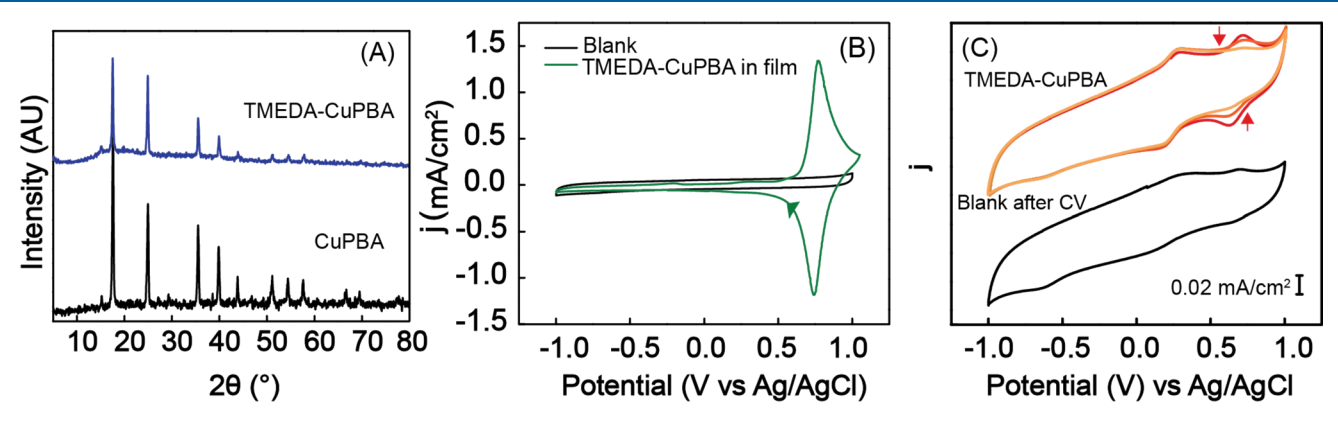


Figure 9. (A) PXRD of CuPBA and TMEDA-CuPBA. (B) CV of TMEDA-CuPBA (cycle 2) immobilized into a C black/Nafion film with 1 M KCl as the supporting electrolyte at 100 mV/s. (C) CV of 1 mg/mL TMEDA-CuPBA suspension in pH 4 buffer containing potassium hydrogen phthalate at 100 mV/s (cycles 2, 5, 10, and 25 are shown) and CV after rinsing the working electrode and placing in a fresh buffer solution containing no TMEDA-CuPBA.

ratio of 2:1 (Figure 8). This material was independently prepared from monomers as reported by Luo et al., following a unique synthesis summarized in Figure 3 as route i. 34 We were also able to obtain the same crystal structure from a third route using an aqueous mixture of the mononuclear complexes $K_4[Fe(CN)_6]$ and $[Cu(OH_2)Cl(en)_2]Cl$ (Figure 3, route iii). Similar to the conversion of Fe(III) in the original CuPBA structure to Fe(II) in the $[Cu(en)_2]^{m+}/[Fe(CN)_6]^{n-}$ and thereby in Cu₂Fe-1D, this previous report also contains Fe(II) in the 1D polymer chain despite starting with $K_3[Fe(CN)_6]$. This reduction has also been observed for other reactions using ferrocyanide with Cu and even Ni mononuclear complexes.³ The exact reason for this reduction is unclear. One report implicates the aqueous medium, while another invokes free cyanide from ferrocyanide, reducing Cu(II) centers into Cu(I), which in turn reduce $[Fe(CN)_6]^{3-}$ to $[Fe(CN)_6]^{4-.35b,36}$ In addition, the FTIR spectrum of $[Cu(en)_2]^{m+}/[Fe(CN)_6]^{n-}$ showed a single CN stretch, while that of Cu₂Fe-1D showed two, which can be attributed to the local D_{4h} symmetry at the Fe centers in the 1D polymer chain, whereas hexacyanoferrate has a local O_h symmetry (Figure S16).

 $[Cu(en)_2]^{m+1}/[Fe(CN)_6]^{n-1}$ was immobilized with carbon black and Nafion to probe the redox response of the material

in a heterogeneous film. As shown in Figure S17, the redox response was similar to that of $[Fe(CN)_6]^{4-}$. The current response decreased with each cycle, which is consistent with the active material dissolving back into the aqueous supporting electrolyte solution. Additionally, the crystals dissolve in water to give a bright purple solution when KCl is added. ICP-MS analysis showed that the Fe–Cu ratio was similar in CuPBA and $[Cu(en)_2]^{m+}/[Fe(CN)_6]^{n-}$ (1.1 and 1.2 respectively).

TMEDA-CuPBA. Since the functionalization of PB with amines tended to result in decomposition, we wondered if our first two amines were simply too effective as ligands for Cu. As such, we wanted to attenuate the donor properties of the amine and decided to try tetramethylethylenediamine. PXRD data showed that with TMEDA, the CuPBA network structure remained intact unlike with propylamine and ethylenediamine (Figure 9A). Similar to [Cu_aFe_bpa_x]_n, the TMEDA-CuPBA suspension in 1 M KCl also showed a color change from dark purple to dark brown within a period of 30 min but did not precipitate to the same extent (Figure S19). If KCl was not present, the TMEDA-CuPBA remained suspended and no color change was observed. Since the changes with KCl were slow, we were able to investigate the initial functionalization product by CV (see Figure S19). We observed a response

consistent with [Fe(CN)₆]³⁻. Although the electrode had no apparent change in appearance after 25 cycles, it was placed in a CuPBA-free fresh electrolyte solution to check for a response that would indicate a persistent film. A redox response was observed for Fe(III/II) in CuPBA and it decreased in intensity with each cycle (see Figures S20 and S21). If the material that precipitated was collected by centrifugation, dried, and immobilized in a carbon black/Nafion film, we observed the same redox response as that observed for Fe(III/II) couple in CuPBA (see Figure 9B). The PXRD data for the material that deposits show the same features as the data for samples of asprepared CuPBA, supporting that the framework is preserved (see Figure S22). Reports show that CuPBA is prone to decomposition at higher pH values.³⁷ Therefore, we explored if a lower pH had any influence of colloidal stability and/or redox activity by carrying out CV experiments at pH 4 using a buffer solution of potassium hydrogen phthalate. Under these conditions, the colloid is prone to aggregate over the course of ~15 min, which is much faster than the aggregation that occurs in 1 M KCl. Although not stable, we notably observed a redox response for the Fe(III/II) associated with the CuPBA network, along with some signals from $[Fe(CN)_6]^{3-}$ (see Figure 9C). While the redox response for $[Fe(CN)_6]^{3-}$ remained constant throughout 25 cycles, the current response for Fe(III/II) from CuPBA decreased with each cycle, as may be expected if the redox-active material is no longer wellsuspended, whereas the $[Fe(CN)_6]^{3-}$ remains dissolved. When the glassy carbon working electrode was rinsed and placed in fresh buffer solution with no TMEDA-CuPBA present, no significant response was observed. This supports that the Fe(III/II) response from TMEDA-CuPBA in pH 4 buffer is caused by the bulk suspension and not from a film, which would have persisted in the fresh electrolyte control experiment.

These results suggest that (1) the TMEDA does not cause the CuPBA network to decompose; (2) over time in KCl, some Fe monomer is extracted, perhaps due to stabilization of monomers by chloride; (3) the TMEDA-CuPBA appears to be redox-active in 1 M KCl but electron transfer again occurs only once it is affixed to the electrode; (4) colloidal TMEDA-CuPBA is redox-accessible at pH 4, but the colloidal stability suffers under these conditions.

CONCLUSIONS

We hypothesized that solubilized PB may be redox-active in suspensions and thus a candidate as the active species for flow battery applications. However, the lack of redox response from insoluble and soluble PB prompted us to study its Cu analogue. The redox response we saw for a suspension of CuPBA in 1 M KCl was a result of a film adsorbed on to the electrode surface, rather than from freely diffusing CuPBA nanoparticles. The film formation on electrodes was further confirmed by bulk electrolysis experiments and SEM. Functionalization of the nanoparticles was explored as a method to prevent film formation of CuPBA. Propylamine modification caused the CuPBA to lose its network structure, confirmed by PXRD, and the redox response observed corresponded to hexacyanoferrate(II) and not to CuPBA. When ethylenediamine was used, the CuPBA network structure dissociated, resulting in a mixture of Cu and Fe mononuclear complexes ($[Cu(en)_2]^{m+}/[Fe(CN)_6]^{n-}$), and in the absence of chloride, a 1D polymer chain formed. When TMEDA was used, the CuPBA network was preserved.

Although electron transfer to or from bulk suspensions of TMEDA-CuPBA in 1 M KCl was not observed, immobilized films of this material were redox-active. Under buffered pH 4 conditions, the TMEDA-CuPBA colloid had a redox response we attribute to the Fe(III/II) couple, although the suspension did not remain well dispersed for longer than 15 min. Since we were able to identify an amine modification that maintained the framework and that pH plays a role in the redox activity, work is ongoing to exploit this strategy and to better understand the role of counterions and supporting electrolyte on charge transfer in these systems.

ASSOCIATED CONTENT

Solution Supporting Information

The Supporting Information is available free of charge at https://pubs.acs.org/doi/10.1021/acs.inorgchem.2c03545.

PXRD; SEM; DLS; FTIR; CVs; bulk electrolysis; scan rate study data; and crystallographic data tables (PDF)

Accession Codes

CCDC 2184756 contains the supplementary crystallographic data for this paper. These data can be obtained free of charge via www.ccdc.cam.ac.uk/data_request/cif, or by emailing data_request@ccdc.cam.ac.uk, or by contacting The Cambridge Crystallographic Data Centre, 12 Union Road, Cambridge CB2 1EZ, UK; fax: +44 1223 336033.

AUTHOR INFORMATION

Corresponding Author

Timothy R. Cook — Department of Chemistry, University at Buffalo, The State University of New York, Buffalo, New York 14260-3000, United States; orcid.org/0000-0002-7668-8089; Email: trcook@buffalo.edu

Authors

Heshali K. Welgama – Department of Chemistry, University at Buffalo, The State University of New York, Buffalo, New York 14260-3000, United States; orcid.org/0000-0002-9826-9803

Matthew R. Crawley – Department of Chemistry, University at Buffalo, The State University of New York, Buffalo, New York 14260-3000, United States; orcid.org/0000-0002-2555-9543

James R. McKone — Department of Chemical and Petroleum Engineering, Swanson School of Engineering, University of Pittsburgh, Pittsburgh, Pennsylvania 15261, United States; orcid.org/0000-0001-6445-7884

Complete contact information is available at: https://pubs.acs.org/10.1021/acs.inorgchem.2c03545

Funding

This work was supported by NSF CBET Awards 2015723 (TRC) and 2015859 (JRM).

Notes

The authors declare the following competing financial interest(s): JRM is named as an inventor on several patents and pending patent applications related to flowable energy storage technologies.

ACKNOWLEDGMENTS

The authors thank Dr. Samantha N. MacMillan for collecting crystallographic data reported in this paper and Dr. Ellen Matson for insightful discussions. This research used resources

in the Chemistry Instrument Center (CIC), Materials Characterization Laboratory (MCL), and the Cleanroom in the University at Buffalo.

REFERENCES

- (1) (a) Wagemaker, M.; Mulder, F. M. Properties and promises of nanosized insertion materials for Li-ion batteries. Acc. Chem. Res. 2013, 46, 1206-1215. (b) Kong, F.; Wang, J.; Han, Z.; Qian, B.; Tao, S.; Luo, H.; Gao, L. Lithium storage mechanisms of CdSe nanoparticles with carbon modification for advanced lithium ion batteries. Chem. Commun. 2019, 55, 2996-2999. (c) Deng, C.; Ma, C.; Lau, M. L.; Skinner, P.; Liu, Y.; Xu, W.; Zhou, H.; Ren, Y.; Yin, Y.; Williford, B.; Dahl, M.; Xiong, H. . C. Amorphous and crystalline TiO2 nanoparticle negative electrodes for sodium-ion batteries. Electrochim. Acta 2019, 321, No. 134723. (d) Chen, H.; Wang, C.; Dong, W.; Lu, W.; Du, Z.; Chen, L. Monodispersed sulfur nanoparticles for lithium-sulfur batteries with theoretical performance. Nano Lett. 2015, 15, 798-802. (e) Tang, B.; Huang, S.; Fang, Y.; Hu, J.; Malonzo, C.; Truhlar, D. G.; Stein, A. Mechanism of electrochemical lithiation of a metal-organic framework without redox-active nodes. J. Chem. Phys. 2016, 144, 194702.
- (2) (a) Wessells, C. D.; McDowell, M. T.; Peddada, S. V.; Pasta, M.; Huggins, R. A.; Cui, Y. Tunable reaction potentials in open framework nanoparticle battery electrodes for grid-scale energy storage. ACS Nano 2012, 6, 1688–1694. (b) Wang, J. Z.; Zhong, C.; Wexler, D.; Idris, N. H.; Wang, Z. X.; Chen, L. Q.; Liu, H. K. Graphene-encapsulated Fe3O4 nanoparticles with 3D laminated structure as superior anode in lithium ion batteries. Chem. Eur. J. 2011, 17, 661–667. (c) Ghosh, S.; Kumar, V. K.; Kumar, S. K.; Biswas, S.; Martha, S. K. An insight of sodium-ion storage, diffusivity into TiO2 nanoparticles and practical realization to sodium-ion full cell. Electrochim. Acta 2019, 316, 69–78.
- (3) Wang, Y.; Li, H.; He, P.; Hosono, E.; Zhou, H. Nano active materials for lithium-ion batteries. *Nanoscale* **2010**, *2*, 1294–1305.
- (4) Sánchez-Díez, E.; Ventosa, E.; Guarnieri, M.; Trovò, A.; Flox, C.; Marcilla, R.; Soavi, F.; Mazur, P.; Aranzabe, E.; Ferret, R. Redox flow batteries: Status and perspective towards sustainable stationary energy storage. *J. Power Sources* **2021**, *481*, No. 228804.
- (5) (a) Montoto, E. C.; Nagarjuna, G.; Hui, J.; Burgess, M.; Sekerak, N. M.; Hernández-Burgos, K.; Wei, T.-S.; Kneer, M.; Grolman, J.; Cheng, K. J.; Lewis, J. A.; Moore, J. S.; Rodríguez-López, J. Redox Active Colloids as Discrete Energy Storage Carriers. *J. Am. Chem. Soc.* **2016**, 138, 13230–13237. (b) Burgess, M.; Moore, J. S.; Rodríguez-López, J. Redox active polymers as soluble nanomaterials for energy storage. *Acc. Chem. Res.* **2016**, 49, 2649–2657.
- (6) Hatakeyama-Sato, K.; Nagano, T.; Noguchi, S.; Sugai, Y.; Du, J.; Nishide, H.; Oyaizu, K. Hydrophilic Organic Redox-Active Polymer Nanoparticles for Higher Energy Density Flow Batteries. *ACS Appl. Polym. Mater.* **2019**, *1*, 188–196.
- (7) Hamelet, S.; Tzedakis, T.; Leriche, J.-B.; Sailler, S.; Larcher, D.; Taberna, P.-L.; Simon, P.; Tarascon, J.-M. Non-aqueous Li-based redox flow batteries. *J. Electrochem. Soc.* **2012**, *159*, A1360.
- (8) (a) Duduta, M.; Ho, B.; Wood, V. C.; Limthongkul, P.; Brunini, V. E.; Carter, W. C.; Chiang, Y. M. Semi-solid lithium rechargeable flow battery. *Adv. Energy Mater.* **2011**, *1*, 511–516. (b) Fan, F. Y.; Woodford, W. H.; Li, Z.; Baram, N.; Smith, K. C.; Helal, A.; McKinley, G. H.; Carter, W. C.; Chiang, Y.-M. Polysulfide flow batteries enabled by percolating nanoscale conductor networks. *Nano Lett.* **2014**, *14*, 2210–2218.
- (9) (a) Sen, S.; Chow, C.-M.; Moazzen, E.; Segre, C. U.; Timofeeva, E. V. Electroactive nanofluids with high solid loading and low viscosity for rechargeable redox flow batteries. *J. Appl. Electrochem.* **2017**, *47*, 593–605. (b) Timofeeva, E. V.; Katsoudas, J. P.; Segre, C. U.; Singh, D. Rechargeable nanofluid electrodes for high energy density flow battery. *In NSTI-Nanotech.* **2013**, *2*, 679–682. (c) Dubal, D. P.; Gomez-Romero, P. Electroactive graphene nanofluids for fast energy storage. *2D Mater.* **2016**, *3*, No. 031004.

- (10) (a) Pan, F.; Yang, J.; Huang, Q.; Wang, X.; Huang, H.; Wang, Q. Redox Targeting of Anatase TiO2 for Redox Flow Lithium-Ion Batteries. *Adv. Energy Mater.* **2014**, *4*, No. 1400567. (b) Huang, Q.; Li, H.; Grätzel, M.; Wang, Q. Reversible chemical delithiation/lithiation of LiFePO 4: towards a redox flow lithium-ion battery. *Phys. Chem. Chem. Phys.* **2013**, *15*, 1793–1797.
- (11) (a) Fan, L.; Jia, C.; Zhu, Y. G.; Wang, Q. Redox targeting of prussian blue: Toward low-cost and high energy density redox flow battery and solar rechargeable battery. ACS Energy Lett. 2017, 2, 615–621. (b) Zanzola, E.; Gentil, S.; Gschwend, G.; Reynard, D.; Smirnov, E.; Dennison, C.; Girault, H. H.; Peljo, P. Solid electrochemical energy storage for aqueous redox flow batteries: The case of copper hexacyanoferrate. Electrochim. Acta 2019, 321, No. 134704. (c) Ostrander, J.; Younesi, R.; Mogensen, R. High Voltage Redox-Meditated Flow Batteries with Prussian Blue Solid Booster. Energies 2021, 14, 7498.
- (12) Ishizaki, M.; Kanaizuka, K.; Abe, M.; Hoshi, Y.; Sakamoto, M.; Kawamoto, T.; Tanaka, H.; Kurihara, M. Preparation of electrochromic Prussian blue nanoparticles dispersible into various solvents for realisation of printed electronics. *Green Chem.* **2012**, *14*, 1537—1544.
- (13) (a) Kraft, A. What a chemistry student should know about the history of Prussian blue. *ChemTexts* **2018**, *4*, 16. (b) Frisch, J. Notitia cœrulei Berolinensis nuper inventi. *Miscnea Berol. Soc. Sci.* **1710**, *1710*, 377–378. (c) Larionova, J.; Guari, Y.; Sangregorio, C.; Guérin, C. Cyano-bridged coordination polymer nanoparticles. *New J. Chem.* **2009**, 33, 1177–1190.
- (14) (a) Ivanov, V. D. Four decades of electrochemical investigation of Prussian blue. *Ionics* **2020**, *26*, 531–547. (b) Kraft, A. Some considerations on the structure, composition, and properties of Prussian blue: A contribution to the current discussion. *Ionics* **2021**, 27, 2289–2305.
- (15) Samain, L.; Grandjean, F.; Long, G. J.; Martinetto, P.; Bordet, P.; Strivay, D. Relationship between the Synthesis of Prussian Blue Pigments, Their Color, Physical Properties, and Their Behavior in Paint Layers. *J. Phys. Chem. C* **2013**, *117*, 9693–9712.
- (16) (a) Ellis, D.; Eckhoff, M.; Neff, V. Electrochromism in the mixed-valence hexacyanides. 1. Voltammetric and spectral studies of the oxidation and reduction of thin films of Prussian blue. *J. Phys. Chem.* **1981**, 85, 1225–1231. (b) Itaya, K.; Ataka, T.; Toshima, S. Spectroelectrochemistry and electrochemical preparation method of Prussian blue modified electrodes. *J. Am. Chem. Soc.* **1982**, 104, 4767–4772.
- (17) Baggio, B. F.; Vicente, C.; Pelegrini, S.; Pla Cid, C. C.; Brandt, I. S.; Tumelero, M. A.; Pasa, A. A. Morphology and structure of electrodeposited Prussian Blue and Prussian white thin films. *Materials* **2019**, *12*, 1103.
- (18) (a) Neff, V. D. Electrochemical oxidation and reduction of thin films of Prussian blue. J. Electrochem. Soc. 1978, 125, 886. (b) Lundgren, C.; Murray, R. W. Observations on the composition of Prussian blue films and their electrochemistry. Inorg. Chem. 1988, 27, 933-939. (c) Orellana, M.; Arriola, P.; Del Río, R.; Schrebler, R.; Cordova, R.; Scholz, F.; Kahlert, H. Chronocoulometric study of the electrochemistry of Prussian blue. J. Phys. Chem. B 2005, 109, 15483-15488. (d) Zakharchuk, N. F.; Meyer, B.; Henning, H.; Scholz, F.; Jaworksi, A.; Stojek, Z. A comparative study of Prussian-Bluemodified graphite paste electrodes and solid graphite electrodes with mechanically immobilized Prussian Blue. J. Electroanal. Chem. 1995, 398, 23-35. (e) Feldman, B.; Murray, R. W. Electron diffusion in wet and dry Prussian blue films on interdigitated array electrodes. Inorg. Chem. 1987, 26, 1702-1708. (f) Feldman, B.; Melroy, O. Ion flux during electrochemical charging of Prussian Blue films. J. Electroanal. Chem. Interfacial Electrochem. 1987, 234, 213-227. (g) Lamprecht, X.; Speck, F.; Marzak, P.; Cherevko, S.; Bandarenka, A. S. Electrolyte Effects on the Stabilization of Prussian Blue Analogue Electrodes in Aqueous Sodium-Ion Batteries. ACS Appl. Mater. Interfaces 2022, 14, 3515-3525. (h) Liu, S.-Q.; Xu, J.-J.; Chen, H.-Y. Electrochemical behavior of nanosized Prussian blue self-assembled on Au electrode surface. Electrochem. Commun. 2002, 4, 421-425. (i) Kulesza, P. J.

- Solid-state electrochemistry of iron hexacyanoferrate (Prussian Blue type) powders: evidence for redox transitions in mixed-valence ionically conducting microstructures. *J. Electroanal. Chem. Interfacial Electrochem.* **1990**, 289, 103–116. (j) Garcia-Jareno, J.; Navarro, J.; Roig, A.; Scholl, H.; Vicente, F. Impedance analysis of Prussian Blue films deposited on ITO electrodes. *Electrochim. Acta* **1995**, 40, 1113–1119.
- (19) (a) Zhou, P.; Xue, D.; Luo, H.; Chen, X. Fabrication, structure, and magnetic properties of highly ordered Prussian blue nanowire arrays. *Nano Lett.* **2002**, *2*, 845–847. (b) Culp, J. T.; Park, J.-H.; Frye, F.; Huh, Y.-D.; Meisel, M. W.; Talham, D. R. Magnetism of metal cyanide networks assembled at interfaces. *Coord. Chem. Rev.* **2005**, 249, 2642–2648.
- (20) (a) Itaya, K.; Shibayama, K.; Akahoshi, H.; Toshima, S. Prussian-blue-modified electrodes: An application for a stable electrochromic display device. *J. Appl. Phys.* **1982**, *53*, 804–805. (b) Cheng, K.-C.; Chen, F.-R.; Kai, J.-J. Electrochromic property of nano-composite Prussian Blue based thin film. *Electrochim. Acta* **2007**, *52*, 3330–3335. (c) Liao, T.-C.; Chen, W.-H.; Liao, H.-Y.; Chen, L.-C. Multicolor electrochromic thin films and devices based on the Prussian blue family nanoparticles. *Sol. Energy Mater. Sol. Cells* **2016**, *145*, 26–34.
- (21) (a) Itaya, K.; Shoji, N.; Uchida, I. Catalysis of the reduction of molecular oxygen to water at Prussian blue modified electrodes. *J. Am. Chem. Soc.* 1984, 106, 3423–3429. (b) Dong, S.; Che, G. Electrocatalytic oxidation of ascorbic acid at a prussian blue film modified microdisk electrode. *J. Electroanal. Chem. Interfacial Electrochem.* 1991, 315, 191–199. (c) Li, J.; Li, Y.; Zhang, Y.; Wei, G. Highly sensitive molecularly imprinted electrochemical sensor based on the double amplification by an inorganic prussian blue catalytic polymer and the enzymatic effect of glucose oxidase. *Anal. Chem.* 2012, 84, 1888–1893.
- (22) (a) Zhang, C.; Xu, Y.; Zhou, M.; Liang, L.; Dong, H.; Wu, M.; Yang, Y.; Lei, Y. Potassium Prussian blue nanoparticles: a low-cost cathode material for potassium-ion batteries. Adv. Funct. Mater. 2017, 27, No. 1604307. (b) Xia, M.; Zhang, X.; Liu, T.; Yu, H.; Chen, S.; Peng, N.; Zheng, R.; Zhang, J.; Shu, J. Commercially available Prussian blue get energetic in aqueous K-ion batteries. Chem. Eng. J. 2020, 394, No. 124923. (c) Zhou, L.; Zhang, M.; Wang, Y.; Zhu, Y.; Fu, L.; Liu, X.; Wu, Y.; Huang, W. Cubic Prussian blue crystals from a facile one-step synthesis as positive electrode material for superior potassium-ion capacitors. Electrochim. Acta 2017, 232, 106-113. (d) Lu, Y.; Wang, L.; Cheng, J.; Goodenough, J. B. Prussian blue: a new framework of electrode materials for sodium batteries. Chem. Commun. 2012, 48, 6544-6546. (e) Ning, F.; Shao, M.; Xu, S.; Fu, Y.; Zhang, R.; Wei, M.; Evans, D. G.; Duan, X. TiO 2/graphene/ NiFe-layered double hydroxide nanorod array photoanodes for efficient photoelectrochemical water splitting. Energy Environ. Sci. 2016, 9, 2633-2643. (f) Peng, Y.; Li, B.; Wang, Y.; He, X.; Huang, J.; Zhao, J. Prussian blue: a potential material to improve the electrochemical performance of lithium-sulfur batteries. ACS Appl. Mater. Interfaces 2017, 9, 4397-4403. (g) Ishizaki, M.; Ando, H.; Yamada, N.; Tsumoto, K.; Ono, K.; Sutoh, H.; Nakamura, T.; Nakao, Y.; Kurihara, M. Redox-coupled alkali-metal ion transport mechanism in binder-free films of Prussian blue nanoparticles. J. Mater. Chem. A 2019, 7, 4777-4787. (h) Xu, Y.; Zheng, S.; Tang, H.; Guo, X.; Xue, H.; Pang, H. Prussian blue and its derivatives as electrode materials for electrochemical energy storage. Energy Storage Mater. 2017, 9, 11-
- (23) (a) Chu, Z.; Liu, Y.; Jin, W. Recent progress in Prussian blue films: Methods used to control regular nanostructures for electrochemical biosensing applications. *Biosens. Bioelectron.* **2017**, *96*, 17–25. (b) Jiang, Y.; Yang, Y.; Shen, L.; Ma, J.; Ma, H.; Zhu, N. Recent Advances of Prussian Blue-Based Wearable Biosensors for Healthcare. *Anal. Chem.* **2022**, *94*, 297–311. (c) Li, J.; Peng, T.; Peng, Y. A cholesterol biosensor based on entrapment of cholesterol oxidase in a silicic sol-gel matrix at a prussian blue modified electrode. *Electroanal.: Int. J. Devoted Fundam. Pract. Aspects Electroanal.* **2003**, *15*, 1031–1037. (d) Jansod, S.; Cherubini, T.; Soda, Y.; Bakker, E. Optical

- sensing with a potentiometric sensing array by Prussian blue film integrated closed bipolar electrodes. *Anal. Chem.* **2020**, *92*, 9138–9145. (e) Du, D.; Wang, M.; Qin, Y.; Lin, Y. One-step electrochemical deposition of Prussian Blue—multiwalled carbon nanotube nanocomposite thin-film: preparation, characterization and evaluation for H2O2 sensing. *J. Mater. Chem.* **2010**, *20*, 1532–1537.
- (24) (a) Yamashita, A.; Sasaki, T.; Tanaka, S. Electrochemical synthesis and immobilization of a beadwork-like Prussian Blue on carbon fiber and the removal of cesium. *J. Environ. Chem. Eng.* **2017**, *5*, 2912–2920. (b) Pandey, P. C.; Yadav, H. P.; Shukla, S.; Narayan, R. J. Electrochemical Sensing and Removal of Cesium from Water Using Prussian Blue Nanoparticle-Modified Screen-Printed Electrodes. *Chemosensors* **2021**, *9*, 253.
- (25) Holdynski, M.; Dolinska, J.; Opallo, M. Collisions of suspended Prussian Blue nanoparticles with a rotating disc electrode. *Electrochem. Commun.* **2018**, *86*, 130–134.
- (26) Cisternas, R.; Muñoz, E.; Henríquez, R.; Córdova, R.; Kahlert, H.; Hasse, U.; Scholz, F. Irreversible electrostatic deposition of Prussian blue from colloidal solutions. *J. Solid State Electrochem.* **2011**, 15, 2461–2468.
- (27) Oldacre, A. N.; Crawley, M. R.; Friedman, A. E.; Cook, T. R. Tuning the Activity of Heterogeneous Cofacial Cobalt Porphyrins for Oxygen Reduction Electrocatalysis through Self-Assembly. *Chem. Eur. J.* **2018**, *24*, 10984–10987.
- (28) Wessells, C. D.; Huggins, R. A.; Cui, Y. Copper hexacyanoferrate battery electrodes with long cycle life and high power. *Nat. Commun.* **2011**, *2*, 550.
- (29) Nishat, N.; Asma; Manisha. Synthesis, characterization, and preliminary antimicrobial evaluation of bisphenol-A formaldehyde resin coordinated with transition metal complexes of ethylenediamine. *J. Appl. Polym. Sci.* **2011**, *119*, 1251–1258.
- (30) (a) Wessells, C. D.; Huggins, R. A.; Cui, Y. Copper hexacyanoferrate battery electrodes with long cycle life and high power. *Nat. Commun.* **2011**, *2*, 550. (b) Makowski, O.; Stroka, J.; Kulesza, P. J.; Malik, M. A.; Galus, Z. Electrochemical identity of copper hexacyanoferrate in the solid-state: evidence for the presence and redox activity of both iron and copper ionic sites. *J. Electroanal. Chem.* **2002**, *532*, 157–164.
- (31) Bard, A. J.; Faulkner, L. R.; White, H. S. Electrochemical methods: fundamentals and applications; John Wiley & Sons, 2022.
- (32) Pasta, M.; Wessells, C. D.; Liu, N.; Nelson, J.; McDowell, M. T.; Huggins, R. A.; Toney, M. F.; Cui, Y. Full open-framework batteries for stationary energy storage. *Nat. Commun.* **2014**, *5*, 3007. (33) Lever, A. B.; Mantovani, E. Far-infrared and electronic spectra
- of some bis (ethylenediamine) and related complexes of copper (II) and the relevance of these data to tetragonal distortion and bond strengths. *Inorg. Chem.* **1971**, *10*, 817–826.
- (34) Luo, J.; Hong, M.; Chen, C.; Wu, M.; Gao, D. Synthesis, magnetic properties and crystal structures of two compounds: [Cu(en)(H2O)]2[Fe(CN)6]·4H2O and [Cu(en)2][KFe(CN)6] (en=ethylenediamine). *Inorg. Chim. Acta* **2002**, 328, 185–190.
- (35) (a) Parker, R. J.; Hockless, D. C.; Moubaraki, B.; Murray, K. S.; Spiccia, L. Hexacyanometalates as templates for heteropolynuclear complexes and molecular magnets: synthesis and crystal structure of [Fe {(CN) Cu (tpa)} 6][ClO 4] 8· 3H 2 O,[tpa= tris (2-pyridylmethyl) amine]. Chem. Commun. 1996, 24, 2789–2790. (b) Parker, R. J.; Spiccia, L.; Moubaraki, B.; Murray, K. S.; Hockless, D. C.; Rae, A. D.; Willis, A. C. Structure and magnetism of heptanuclear complexes formed on encapsulation of hexacyanoferrate (II) with the Mn (II) and Ni (II) complexes of 1, 4-bis (2-pyridylmethyl)-1, 4, 7-triazacyclononane. Inorg. Chem. 2002, 41, 2489–2495. (c) Koo, J.-E.; Kim, D.-H.; Kim, Y.-S.; Do, Y. Cyano-Bridged Homometallic 1-D and Bimetallic 2-D Assemblies: Synthesis, Structures, and Magnetic Properties of [Ni (baepn)(CN)] n (ClO4) n and [Ni (baepn)] 2 n [Fe (CN) 6] n (H2O) 8 n. Inorg. Chem. 2003, 42, 2983–2987.
- (36) Triki, S.; Sala-Pala, J.; Thétiot, F.; Gómez-García, C. J.; Daran, J. C. New, Multi-Dimensional Cu (tn)-[M (CN) 6] n—Cyano-Bridged,

Bimetallic Coordination Materials (M = FeII, CoIII, CrIII and tn= 1, 3-Diaminopropane); Wiley Online Library , 2006.

(37) Shi, L.; Newcomer, E.; Son, M.; Pothanamkandathil, V.; Gorski, C. A.; Galal, A.; Logan, B. E. Metal-ion depletion impacts the stability and performance of battery electrode deionization over multiple cycles. *Environ. Sci. Technol.* **2021**, *55*, 5412–5421.

□ Recommended by ACS

Au/Pd Nanocatalysts on Silica Nanoparticle-Coated Indium Tin Oxide for Colorimetric Sensing of Ascorbic Acid

Ridge Chavalala and Philani Mashazi

DECEMBER 27, 2022

ACS APPLIED NANO MATERIALS

READ 🗹

NO and N₂O Release from the Trityl Diazeniumdiolate Complexes $[M(O_2N,CPh_3)_3]^-(M=Fe,Co)$

Miguel Á. Baeza Cinco, Trevor W. Hayton, et al.

MARCH 13, 2023

INORGANIC CHEMISTRY

READ 🗹

Syntheses and Structures of Arenethiolato Cobalt(II) Complexes Containing Acylamino Groups: Steric Effects of Bulky Ligands on Coordination and Geometry

Yusuke Tomita, Kiyotaka Onitsuka, et al.

MAY 25, 2023

INORGANIC CHEMISTRY

READ 🗹

Linear, Electron-Rich, Homoleptic Rare Earth Metallocene and Its Redox Activity

Ernesto Castellanos and Selvan Demir

JANUARY 23, 2023

INORGANIC CHEMISTRY

READ 🗹

Get More Suggestions >